Article

Catalytic activity of peptide-nanoparticle conjugates regulated by a conformational change

Dorian Jamal Mikolajczak, Jason Lee Heier, Boris Schade, and Beate Koksch

Biomacromolecules, **Just Accepted Manuscript** • DOI: 10.1021/acs.biomac.7b00887 • Publication Date (Web): 19 Sep 2017

Catalytic activity of peptide-nanoparticle conjugates regulated by a conformational change

*Dorian J. Mikolajczak[1], Jason L. Heier[1], Boris Schade[2], Beate Koksch[1]**

[1]Freie Universität Berlin Department of Biology, Chemistry and Pharmacy, Institute of Chemistry and Biochemistry, Berlin, Germany

[2]Freie Universität Berlin Department of Biology, Chemistry and Pharmacy, Institute of Chemistry and Biochemistry Research Center for Electron Microscopy, Berlin, Germany

Keywords: catalysis, peptide, gold nanoparticles, self-assembly, nanozymes, regulation

ABSTRACT

Herein, we present the design and synthesis of a catalytically active peptide-nanoparticle conjugate whose activity is regulated by a defined conformational change in the self-assembled peptide monolayer. A catalytically active peptide, designed after the heterodimeric α-helical coiled-coil principle was immobilized onto gold nanoparticles and kinetic studies were performed according to the Michaelis-Menten model. The formed peptide monolayer at the gold nanoparticle surface accelerated *p*-nitrophenylacetate (*p*NPA) hydrolysis by one order of

magnitude compared to the soluble peptide while exhibiting no defined secondary structure as determined by infrared (IR) and circular dichroism (CD) spectroscopy. Addition of the complementary peptide induced coiled-coil formation while significantly hindering the *p*NPA hydrolysis catalyzed by the peptide-nanoparticle conjugate. The heptad repeat sequence of a coiled-coil opens up the opportunity for regulation of conformation and thus catalytic activity of peptide-nanoparticle conjugates upon interaction with a complementary coiled-coil sequence. Strategies of regulation of catalytic activity by interaction with a complementary cofactor/ligand are well-established in nature and are introduced here into rationally designed peptide-nanoparticle conjugates.

INTRODUCTION

The design and creation of nanomolecular systems that mimic the catalytic specificity and efficiency of enzymes have been a great scientific and technological challenge for decades. Intensive research has been promoted to elucidate structural features and complex interactions of enzymes responsible for their unique catalytic and regulatory mechanisms[1,2] in order to develop catalysts with fine-tuned specificity, high turnover rates, and increased robustness, that are also easily prepared and applied.[3]

Among different approaches used to create artificial enzymes,[4–6] the application of gold nanoparticles (Au-NP) conjugated to a monolayer of thiols (Au-MPCs = monolayer protected gold clusters) has proven to be a powerful tool.[7–9] In particular, Au-NPs functionalized with a monolayer of cysteine-containing peptides exhibit exceptional properties in molecular recognition and catalysis.[10,11] The high peptide density surrounding the nanoparticle generates

new microenvironments, which are able to establish new hydrogen bond networks and cooperative effects between residues that are absent when the peptide or peptides are free in solution.[12] As a result, such effects are capable of creating complex environments resembling the active sites of native enzymes. The application of nanoparticles can therefore yield catalytic efficiencies increased by several orders of magnitude over non-conjugated peptide variants, and even generate new catalytic activities, operative under conditions where the monomeric peptide shows no catalytic activity.[12,13] In addition, the monolayer can be designed to further modulate activity by accommodating the lipophilicity of chosen substrate.[13]

The usage of peptide capped Au-MPCs had been "exploited to study confinement and clustering effects on the reactivity of functional groups" in an effort to deepen the understanding of complex interactions of amino acid residues located in catalytic sites.[12] To broaden the knowledge of peptide-capped nanoparticles as a design principle for enzyme mimics, we investigated the peptide structure-function relationship of such systems by means of defined conformational changes and their effect on catalytic activity.

In nature, the catalytic activity of an enzyme is achieved and regulated by its overall protein topology with solvation of particular residues specifically located within its active site. In other words, catalytic activity depends on the appropriate folding of the polypeptide chains into defined three-dimensional structures under specific environmental conditions. In an opposite way, catalytic activity of peptide capped Au-MPCs can be manipulated by forming defined structures within the peptide monolayer. We herein report the design and synthesis of a peptide-

nanoparticle conjugate with esterase properties, whose activity is regulated by a defined conformational change of the peptide monolayer from random into coiled-coil structures.

MATERIALS AND METHODS

Peptide synthesis

Peptides were manually synthesized on TGA resin using standard fluorenylmethyloxycarbonyl (Fmoc) methodology.[14] The coupling procedure of each Fmoc-protected amino acid (5 eq.) was performed twice employing reagents *N,N'*-diisoproplycarbodiimide (DIC) (4.9 eq.) and 1-hydroxy-7-azabenzotriazole (HOAt) (5 eq.) in DMF. Side-chain deprotection and peptide/resin cleavage were accomplished using a cocktail of thioanisole, phenol, triisopropylsilane (TIS), 1,2-ethanedithiol (EDT), H_2O and trifluoroacetic acid (TFA) (5:5:5.2.5:2.5:80, v/v) for peptides containing cysteine and a cocktail of TIS, H_2O and TFA (3:2:95, v/v) for peptides without cysteine. Crude peptides were precipitated in ice-cold diethyl ether and purified via reverse-phase HPLC LaPrep∑ low-pressure HPLC system (VWR, Darmstadt, Germany) using a Kinetex RP-C18 endcapped HPLC-column (5 µM, 100 Å, 250 x 21.2 mm, Phenomenex®, USA). A SecurityGuard™ PREP Cartridge Holder Kit (21.20 mm, ID, Phenomenex®, USA) served as pre-column. As eluents, deionized water (Milli-Q Advantage® A10 Ultrapure Water Purification System, Millipore®, Billerica, MA, USA) and acetonitrile (ACN), both containing 0.1 % (v/v) TFA were used. HPLC runs were performed starting with an isocratic gradient of 5 % ACN over 5 min, flow rate: 10 mL/min, continuing with a linear gradient of 5 – 70 % ACN over 25 min, flow rate: 20.0 mL/min.

Nanoparticle synthesis

An aqueous solution of $HAuCl_4$ (0.2 mL, $2.49 \cdot 10^{-2}$ M) was added to 2 mL of enzyme-free water (EF-H_2O, Water for Molecular Biology, Merck Millipore). Under vigorous stirring, 0.5 mL of aqueous peptide E3H15 ($5.438 \cdot 10^{-4}$ M) solution and 0.03 mL of 1 M NaOH solution were added. Following 30 min of stirring, 0.1 mL aqueous 0.1 M $NaBH_4$ was added and a wine red dispersion was immediately formed. After stirring for an additional 60 min, the dispersion was centrifuged using Amicon Ultra-0.5 centrifugal filters (NMWL 30kDa) to recover a pellet of peptide-capped gold nanoparticles. The pellet was redispersed in EF-H_2O and again centrifuged to remove excess $NaBH_4$. The resulting pellet was redispersed in EF-H_2O and stored at room temperature. Nanoparticle concentration was calculated according to equations provided by Liu *et al.*[15] An average loading of 265 peptides per gold nanoparticle was determined by analyzing the centrifuged supernatants by UV/Vis-spectroscopy using a Cary 50 UV/Vis-spectrometer (Varian) and reverse-phase HPLC. The amount of bound E3H15 was obtained by subtracting the amount of unbound peptide present in the supernatant from the amount of peptide initially used in the synthesis.

Peptide stock solutions

Peptide stock solutions were prepared by dissolving lyophilized peptide in 50 mM Tris/HCl buffer pH 7.3. Concentrations of stock solutions were determined by measuring the UV-light absorbed by a diluted aliquot. Applying the Lambert-Beer law and taking into account dilution factors, concentrations of peptide stock solutions were calculated according to their respective chromophore. For E3H15, an extinction coefficient (ε_{280}) of 1263 L mol^{-1} cm^{-1} was applied, which was experimentally determined by measuring the absorbance of tyrosine in H_2N-CGGYE-OH at 280 nm[16–18] in 50 mM Tris/HCl pH 7.3. For the peptide K3, which contains the

chromophore 2-aminobenzoic acid (Abz), a pre-determined extinction coefficient (ε_{320}) of H_2N-Abz-Gly-OH at 320 nm of 2980 L mol^{-1} cm^{-1} was applied.

Michaelis-Menten kinetic assay

Michaelis-Menten kinetics was applied to assess the rate of hydrolysis of the ester substrate *p*NPA at pH 7.3 (50 mM Tris/HCl) and 25°C. Reactions were monitored by measuring the absorbance of the formed product *p*-nitrophenolate at 405 nm. Using an experimentally determined extinction coefficient of 9919 L mol^{-1} cm^{-1}, initial rates of reaction (v_0) of uncatalyzed (blank) and catalyzed reactions were determined over a range of substrate concentrations until saturation conditions were observed. Initial rates of reaction of the catalyst were obtained by subtracting v_0 of the blank reaction from v_0 of the corresponding catalyzed reaction. All kinetic experiments were performed at least three times to determine standard deviation. The maximum rate of reaction at saturating substrate concentrations v_{max} and the Michaelis constant K_M, which is the substrate concentration at which the rate of the catalyzed reaction is half v_{max}, were obtained by performing a non-linear regression of the Michaelis-Menten equation. Errors were calculated according to error propagation derived from the Gaussian equation for normally distributed errors.

All reactions were performed in quartz QS cuvettes with a 1 cm pathlength and, equipped with Teflon stoppers (3.5 mL; Hellma Analytics) in a UV/Vis-spectrophotometer (Cary 50, Varian) thermostatted at 25° C (Lauda RKS). All solutions used in the reactions were allowed to equilibrate at 25 °C 20 minutes prior to the start of the reaction. These solutions included a stock

solution of *p*NPA dissolved in acetonitrile as well as the reaction cuvette containing only buffer (blank) or peptide dissolved in buffer. Reactions were initiated by adding a volume of substrate solution so the total volume of all reaction mixtures contained 2% acetonitrile. The total solution volume of each reaction was 1 mL.

Kinetic assays with E3H15 were performed in 50 mM Tris/HCl buffer pH 7.3 at 25 °C with a peptide concentration of 50 µM. In these assays, initial *p*NPA concentrations of 0.1, 0.2, 0.5, 1.0, 2.0 and 4.0 mM in the reaction mixture were employed.

Kinetic assays with the synthesized peptide-gold nanoparticle conjugate (Au@E3H15) as well as measurements containing 5 µM K3 were performed in 50 mM Tris/HCl buffer pH 7.3 at 25 °C using a calculated concentration of 5 µM immobilized E3H15 peptide. Initial *p*NPA concentrations of 0.05, 0.075, 0.1, 0.2, 0.3 and 0.5 mM were applied in these reactions.

Circular dichroism (CD) spectroscopy

CD-spectra were obtained using a Jasco J-810 spectropolarimeter with a HAAKE WKL recirculating chiller (D-76227, Karlsruhe). The cuvettes were set to a constant temperature of 25° C with a Jasco PTC-423S Peltier-type thermocouple. Measurements were performed in quartz cuvettes (Suprasil Hellma) having a pathlength of 2 mm.

FT-IR spectroscopy

IR-spectra were recorded using an ATR-FT/IR-4100 by Jasco, averaging 100 scans with 3 cm^{-1} resolution. Lyophilized peptide and peptide-gold nanoparticle conjugates were placed on the diamond crystal. IR-spectra were recorded, taking into account the corresponding background.

Transmission electron microscopy (TEM)

Aliquots (5 µL) of the aqueous samples were applied to a formvar/carbon covered copper grid (400 mesh, PLANO GmbH, Wetzlar) which was hydrophilized by 60 s glow discharging at 8 W in a BALTEC MED 020 device directly before use. After 30 s of AuNP sedimentation excess liquid was removed with filter paper and the grid was allowed to air-dry for at least 20 min. The grid was then transferred to a Tecnai F20 transmission electron microscope (FEI Company, Oregon) equipped with a field emission gun operating at an acceleration voltage of 160 kV. Image data were recorded using a FEI Eagle 4k × 4k CCD camera with a primary magnification of 100,000 x resulting in an image resolution of 0.214 nm/dot of the electron micrographs.

Nanoparticle size and size distribution were determined using ImageJ (Image processing and analysis in JAVA) V 1.50[19] by analyzing at least 1000 particles.

RESULTS AND DISCUSSION

Peptide design

Peptides E3H15 and K3 (Fig. 1) were designed according to the well-characterized IAAL-E3/IAAL-K3 coiled-coil peptide system.[20] Both peptides include the basic principles of a parallel heterodimeric α-helical coiled-coil folding motif. Thus, by combining both peptides, coiled-coil formation is readily induced.

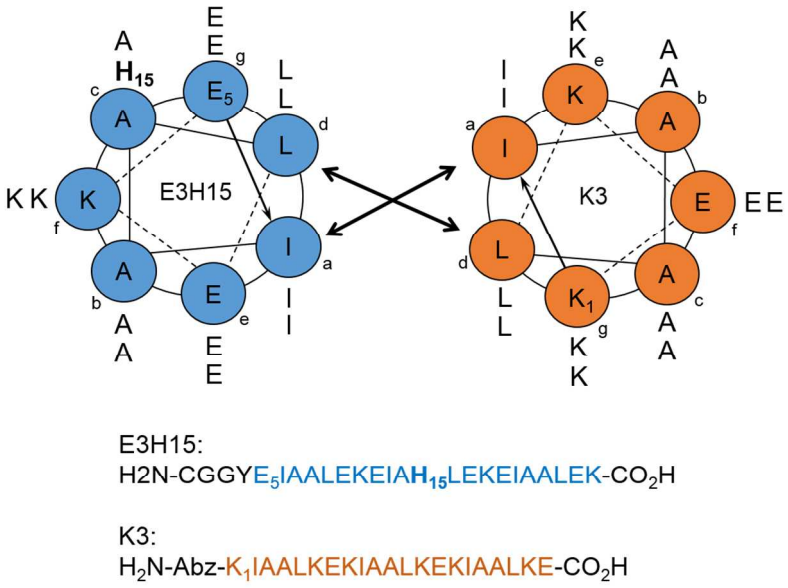

Figure 1. Peptide sequences of E3H15 and K3. Heptad repeat patterns are highlighted in blue (E3H15) and orange (K3) and represented in the helical wheel diagram.

The peptide E3H15 was designed to feature a histidine residue in position 15 among several glutamate residues. Thus, an imidazole moiety is present in a carboxylate-rich environment to create a catalytically active charge-relay network capable of accelerating ester hydrolysis. Furthermore, the generation of cooperative carboxylate-imidazole interactions is likely enhanced when peptides are immobilized as has previously been reported.[12] Covalent attachment of E3H15 onto the gold nanoparticle surface is easily provided by a thiol-gold bond via the *N*-terminal cysteine residue.[21,22]

Preparation and characterization of Au@E3H15

Preparation and functionalization of the gold nanoparticles were performed by reduction of an Au(III) salt by $NaBH_4$ in presence of E3H15, which also acts as a stabilizing ligand. The average size of gold nanoparticles was determined by transmission electron microscopy (TEM).

Concentration of gold nanoparticle dispersion was calculated according to equations reported by Liu *et al.*[23] (Supporting Information). TEM revealed spherical Au@E3H15 particles with an average diameter of 5.4 ± 2.0 nm (Fig. 2).

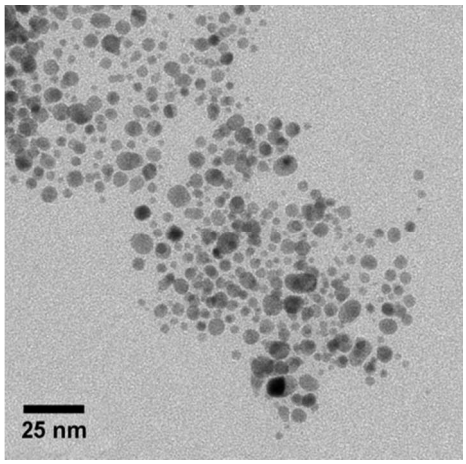

Figure 2. TEM-image of Au@E3H15.

By taking into account the amount of bound peptide as determined by supernatant analysis, the average peptide loading was determined to be 265 peptides per gold nanoparticle.

To confirm peptide binding and to detect changes in the peptide IR spectrum owing to the immobilization process, FT-IR spectroscopy was performed (Fig. 3 A). FT-IR showed the presence of IR stretching frequencies of multiple bands present in E3H15, such as Amide A, Amide I and Amide II. Most strikingly, the Amide A band at 3289 cm^{-1} appears to be significantly broader for Au@E3H15 than for E3H15. This broadening of the Amide A band indicates multiple new hydrogen bond interactions of the N-H groups likely resulting from the increased peptide density at the nanoparticle surface and a close proximity between intermolecular residues.[24] The inability of E3H15 and Au@E3H15 to form defined secondary

structures under the specified conditions was validated by CD spectroscopy (Fig. 3 B), which resulted in spectra having single ellipticity minima at 199 and 191 nm, respectively.

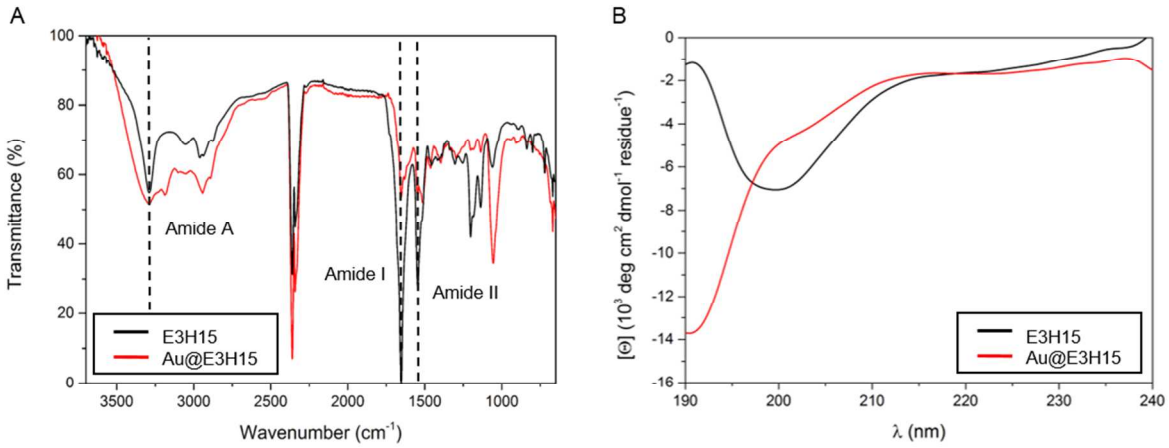

Figure 3. (A) FT-IR spectra of E3H15 and Au@E3H15. (B) Normalized CD spectra of E3H15 and Au@E3H15. CD spectra were recorded at pH 7.3 and 25 °C in 50 mM Tris/HCl-buffer with 2 % acetonitrile and a total peptide concentration of 50 µM.

Effect of immobilization on catalytic efficiency

In the present study, catalyzed ester hydrolysis was accessed using the chromogenic model ester *p*NPA. This ester serves as a benchmark substrate for studying the hydrolytic activity of enzymes[25] and designed peptide catalysts.[26] The dependence of the initial rates of *p*NPA hydrolysis on *p*NPA concentration is in accordance with the Michaelis-Menten model for E3H15 and Au@E3H15. However, due to its low catalytic activity, a minimum concentration of 50 µM E3H15 was needed to clearly observe catalysis. On the other hand, a lower peptide concentration of 5 µM of immobilized E3H15 provided sufficient study of Au@E3H15-catalyzed hydrolysis while avoiding experimental complications caused by the highly absorbent nature of Au-NPs.

Table 1. Kinetic parameters kcat, K_M and kcat/K_M of *p*NPA hydrolysis at 25 °C in Tris/HCl buffer pH 7.3 with 2 % acetonitrile in the presence of 50 µM E3H15 and K3 for E3H15 and E3H15 / K3 and 5 µM immobilized E3H15 and K3 for Au@E3H15 and Au@E3H15 / K3.

Catalyst	k_{cat} [10^{-4} s^{-1}]	K_M [mM]	k_{cat}/K_M [M^{-1} s^{-1}]
E3H15	1.92 ± 0.25	0.98 ± 0.26	0.20 ± 0.08
E3H15 / K3	2.29 ± 0.51	1.49 ± 0.56	0.15 ± 0.09
Au@E3H15	7.20 ± 1.09	0.31 ± 0.09	2.18 ± 0.95
Au@E3H15 / K3	-	-	-

Table 1 shows concentration-independent kinetic parameters k_{cat}, K_M and k_{cat}/K_M. The immobilization of E3H15 onto gold nanoparticles led to an 11-fold increase in catalytic efficiency k_{cat}/K_M. Interestingly, the improvement of catalytic efficiency originates from a decrease in K_M and an increase in turnover number of the catalyst k_{cat}, both by a factor of approximately three. A decrease in K_M indicates an increased binding affinity of *p*NPA for the peptide monolayer of Au@E3H15 compared to the free peptide. This finding could be explained with the formation of transient enzyme-like binding pockets at the Au@E3H15 surface in which the substrate is preferentially bound. Riccardi *et al.* validated the existence of such cavities within self-organized monolayers of thiol-functionalized gold nanoparticles.[27] They showed that Au-NPs functionalized with oligo(ethylene glycol)-based thiols are able to bind and accommodate small organic aromatic molecules such as salicylate in self-organized transient binding pockets within the monolayer with different selectivity and sensitivity similar to protein-ligand recognition. We speculate that such binding processes could also occur within the peptide monolayer of Au@E3H15, leading to the observed decrease in K_M.

The increase in turnover number k_{cat}, which is also the first order rate constant of Au@E3H15 shows that the hydrolytic process in the Au@E3H15 monolayer occurs more rapidly. This can be attributed to an additionally formed cooperative carboxylate-imidazolium mechanism, as proposed by Pengo *et al*.[12,13] The free peptide containing the amphoteric histidine imidazole and carboxylate groups is expected to follow a catalytic general acid and general base mechanism (Scheme 1A) similar to His/Glu or His/Asp dyads in esterases.[28] In case of Au@E3H15, the high local peptide density surrounding the nanoparticle and thus presentation of multiple carboxylate moieties in close proximity to the imidazole can lead to an increase in its pK_a, thus favoring the protonated imidazolium ion. The imidazolium ion, in turn, acts as a general acid, forming a stabilizing hydrogen bond with the developing charge of the subsequent tetrahedral transition state of ester hydrolysis. In this scenario, the tetrahedral transition state is initiated by a carboxylate anion, acting as a general base. This additional cooperative hydrolytic pathway is said to be absent in the monomeric peptide-solution and results in a rate acceleration of the hydrolytic process.[12,13] Another mechanism for the rate acceleration of nucleophilic reactions on carbonyl compounds catalyzed by imidazolium cations was proposed by Ullah *et al*.[29] Thereby, the imidazolium cation interacts with the carbonyl oxygen, activating the carbonyl carbon and facilitating the following nucleophilic attack. Based on the mechanistic proposals we assume the mechanism of *p*NPA hydrolysis catalyzed by Au@E3H15 to be as depicted in Scheme 1B.

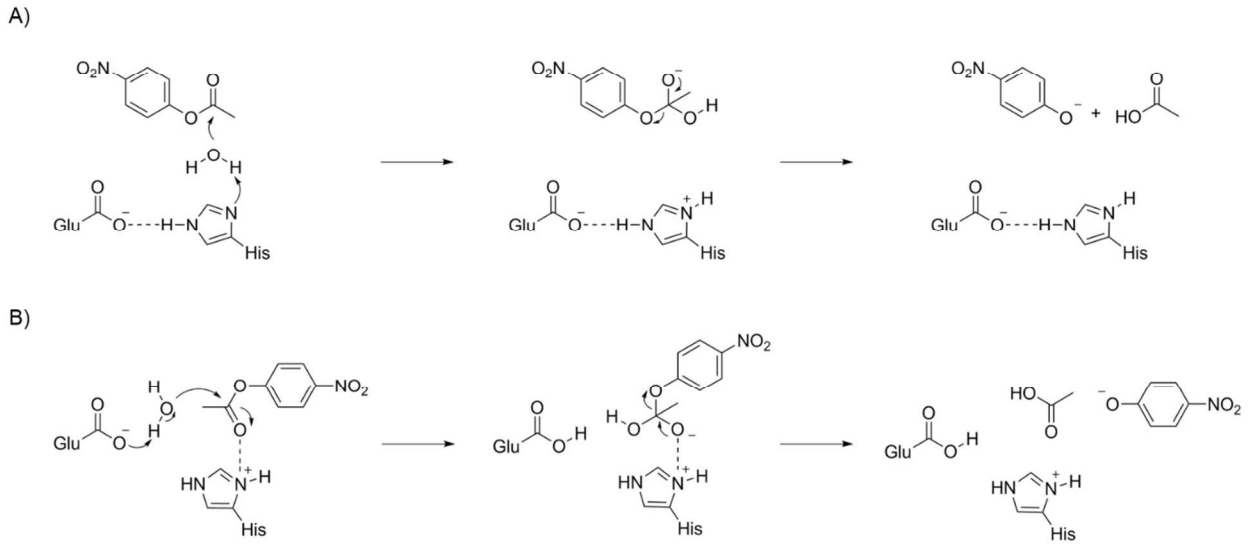

Scheme 1. (A) Proposed mechanism for the hydrolysis of *p*NPA catalyzed by carboxylate anions and imidazole present in E3H15. (B) Proposed mechanism for the hydrolysis of *p*NPA catalyzed by carboxylate anions and imidazolium cations additionally present in the Au@E3H15 monolayer.

Regulation of activity by coiled-coil formation

Having determined the catalytic activity of Au@E3H15, we investigated the effect conformational change has on catalytic activity. By themselves, Au@E3H15 and K3 each showed no defined secondary structures (Fig. 4A). Au@E3H15 when mixed with equimolar K3 resulted in increased α-helical content as observed by CD spectra showing two new minima at 222 nm and 202 nm. By virtue of the chosen peptide design, coiled-coil conformation is likely induced on interaction of E3H15 and K3 and adopted.

Kinetic studies performed on Au@E3H15 in the presence of equimolar K3 revealed an average decrease in catalytic activity of Au@E3H15 by 85 % at all substrate concentrations (Fig. 4B). In contrast, a marginal decrease in catalytic activity was observed for soluble coiled-coil E3H15 in the presence of K3 (Fig. 4C, D).

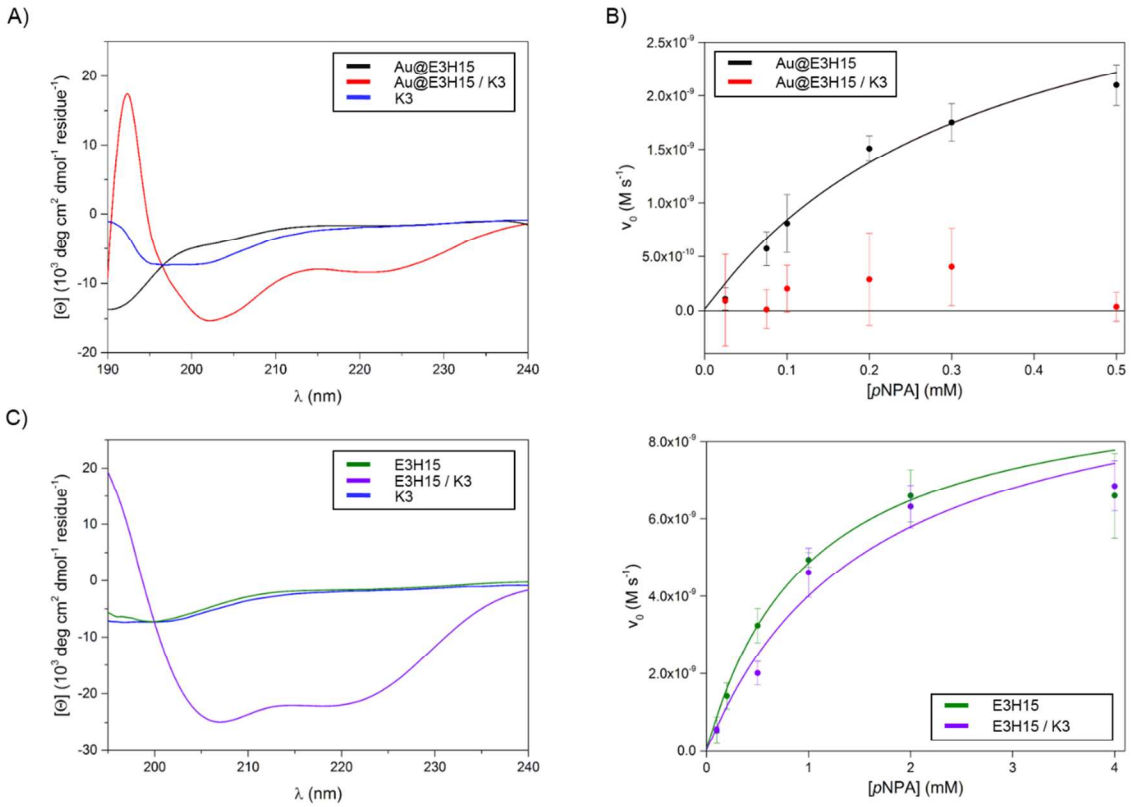

Figure 4. (A) Normalized CD spectra of Au@E3H15, K3 and a mixture of both. (B) Michaelis-Menten plots of blank-corrected *p*NPA hydrolysis catalyzed by Au@E3H15 and Au@E3H15/K3. (C) Normalized CD spectra of E3H15, K3 and a mixture of both. (D) Michaelis-Menten plots of blank-corrected *p*NPA hydrolysis catalyzed by E3H15 and E3H15/K3. Error bars depict standard deviations of at least three independent measurements.

The effective reduction of catalytic efficiency due to interaction with complementary inhibitor K3 in case of Au@E3H15 is most likely due to a combination of several effects. The E3H15 chains are involved in more rigid α-helical coiled-coil structures which hinders the formation of possible binding cavities. The fixed orientation of histidine and glutamate residues within a coiled-coil arrangement leads to reduction of intramolecular cooperative interactions necessary

for substrate activation and stabilization. Furthermore, intercalation of K3 into the E3H15 monolayer can disrupt intermolecular cooperative residue interactions responsible for the increased catalytic efficiency of Au@E3H15. The presence of lysine-rich K3 within the glutamate-rich E3H15 monolayer could also lead to a decreased intrinsic pk_a of the histidine imidazole moiety by electrostatic effects as opposed to the solely E3H15 monolayer. In either case, the additional cooperative mechanism is diminished and catalysis is decreased. Detailed mechanistic studies of Au@E3H15-catalyzed ester hydrolysis and its inhibition by K3 are currently ongoing.

Conclusion

Herein, we report the first example of a peptide-nanoparticle conjugate whose catalytic activity is regulated by a defined change in peptide conformation from random coil to coiled-coil structures. The immobilization of peptide E3H15 onto spherical Au-NPs (Au@E3H15) triggers cooperative glutamate-histidine interactions resulting in an increase in catalytic efficiency of *p*NPA hydrolysis by more than one order of magnitude in comparison to non-immobilized E3H15. Au@E3H15 shows no defined secondary structure as was validated by IR and CD spectroscopy. However, when combined with complementary coiled-coil peptide K3 in equimolar ratios, coiled-coil formation was induced. The generation of rigid coiled-coil structures and the formation of a mixed layer of E3H15 and K3 led to a significant inhibition of catalytic activity. Detailed mechanistic studies of the complex interactions within these peptide monolayers are ongoing.

Our results show the importance peptide topology has on the catalytic activity of peptide-nanoparticle conjugates and present a viable approach towards the design of enzyme mimics with more complex structure-function relationships.

ASSOCIATED CONTENT

Supporting Information

UV/Vis-spectroscopic measurements showing absorbance against time spectra of *p*NPA hydrolysis at different concentrations catalyzed by Au@E3H15. UV/vis-spectrum of Au@E3H15. Calibration curve of *p*NPA blank reactions. Comparison between UV/vis-spectra of H_2N-CGGYE-OH dilution series and supernatant of Au@E3H15 after synthesis. RP-HPLC chromatogram of Au@E3H15 supernatant after synthesis. Equations used to determine gold nanoparticle concentrations.

AUTHOR INFORMATION

Corresponding Author

Beate Koksch, Freie Universität Berlin

Department of Biology, Chemistry, Pharmacy Institute of Chemistry and Biochemistry Berlin, Germany.

Email: beate.koksch@fu-berlin.de

Funding Sources

The authors gratefully thank the Integrated Research Training Group (Graduiertenkolleg) "Multivalency in Chemistry and Biochemistry" of the Collaborative Research Center 765 (SFB 765) "Multivalency as Chemical Organizational and Operational Principle: New Architectures, Functions, and Applications" at the Freie Universitaet Berlin funded by the German Research Foundation (DFG).

REFERENCES

(1) Dong, Z.; Luo, Q.; Liu, J. *Chem. Soc. Rev.* **2012**, *41* (23), 7890–7908.

(2) Wiester, M. J.; Ulmann, P. A.; Mirkin, C. A. *Angew. Chemie - Int. Ed.* **2011**, *50* (1), 114–137.

(3) Stodulski, M. I.; Gulder, T. *Angew. Chemie - Int. Ed.* **2012**, *51* (45), 11202–11204.

(4) Breslow, R. *Acc. Chem. Res.* **1995**, No. 33, 146–153.

(5) Wei, H.; Wang, E. *Chem. Soc. Rev.* **2013**, *42* (14), 6060–6093.

(6) Nanda, V.; Koder, R. L. *Nat. Chem.* **2010**, *2* (1), 15–24.

(7) Pasquato, L.; Pengo, P.; Scrimin, P. *Supramol. Chem.* **2005**, *17* (1–2), 163–171.

(8) Taguchi, T.; Isozaki, K.; Miki, K. *Adv. Mater.* **2012**, *24* (48), 6462–6467.

(9) Pieters, G.; Prins, L. J. *New J. Chem.* **2012**, *36* (10), 1931.

(10) Tauran, Y.; Brioude, A.; Coleman, A. W.; Rhimi, M.; Kim, B. *World J. Biol. Chem.* **2013**, *4* (3), 35–63.

(11) Lévy, R. *ChemBioChem* **2006**, *7* (8), 1141–1145.

(12) Pengo, P.; Polizzi, S.; Pasquato, L.; Scrimin, P. *J. Am. Chem. Soc.* **2005**, *127* (6), 1616–1617.

(13) Pengo, P.; Baltzer, L.; Pasquato, L.; Scrimin, P. *Angew. Chemie - Int. Ed.* **2007**, *46* (3), 400–404.

(14) Fields, G. B.; Noble, R. L. *Int. J. Pept. Protein Res.* **1990**, *35* (3), 161–214.

(15) Liu, X.; Atwater, M.; Wang, J.; Huo, Q. *Colloids Surfaces B Biointerfaces* **2007**, *58* (1), 3–7.

(16) Pace, C. N.; Vajdos, F.; Fee, L.; Grimsley, G.; Gray, T. *Protein Sci.* **1995**, *4* (11), 2411–2423.

(17) Anthis, N. J.; Clore, G. M. *Protein Sci.* **2013**, *22*, 851–858.

(18) Edelhoch, H. *Biochemistry* **1967**, *6* (7), 1948–1954.

(19) Schneider, C. A.; Rasband, W. S.; Eliceiri, K. W. *Nat. Methods* **2012**, *9* (7), 671–675.

(20) Litowski, J. R.; Hodges, R. S. *J. Biol. Chem.* **2002**, *277* (40), 37272–37279.

(21) Serizawa, T.; Hirai, Y.; Aizawa, M. *Langmuir* **2009**, *25* (20), 12229–12234.

(22) Xue, Y.; Li, X.; Li, H.; Zhang, W. *Nat. Commun.* **2014**, *5*, 4348.

(23) Liu, X.; Atwater, M.; Wang, J.; Huo, Q. *Colloids Surfaces B Biointerfaces* **2007**, *58* (1), 3–7.

(24) Porta, F.; Speranza, G.; Krpetić, Ž.; Dal Santo, V.; Francescato, P.; Scarì, G. *Mater. Sci. Eng. B Solid-State Mater. Adv. Technol.* **2007**, *140* (3), 187–194.

(25) Huggins, C.; Lapides, J. *J. Biol. Chem.* **1947**, *170* (2), 467–482.

(26) Rufo, C. M.; Moroz, Y. S.; Moroz, O. V.; Stöhr, J.; Smith, T. a.; Hu, X.; DeGrado, W. F.; Korendovych, I. V. *Nat. Chem.* **2014**, *6* (4), 303–309.

(27) Riccardi, L.; Gabrielli, L.; Sun, X.; De Biasi, F.; Rastrelli, F.; Mancin, F.; De Vivo, M. *Chem* **2017**, *3* (1), 92–109.

(28) Steiner, K.; Schwab, H. *Comput. Struct. Biotechnol. J.* **2012**, *2*, e201209010.

(29) Ullah, B.; Chen, J.; Zhang, Z.; Xing, H.; Yang, Q.; Bao, Z.; Ren, Q. *Sci. Rep.* **2017**, *7*, 42699.

Table of Contents Graphic (TOC)